

available at www.sciencedirect.comjournal homepage: www.elsevier.com/locate/chnjc

Communication

Evolution of catalytic activity driven by structural fusion of icosahedral gold cluster cores



Dan Yang, Yan Zhu *

School of Chemistry and Chemical Engineering, Nanjing University, Nanjing 210093, Jiangsu, China

ARTICLE INFO

Article history:

Received 18 April 2020

Accepted 21 May 2020

Published 5 February 2021

Keywords:

Gold cluster

Structure fusion

Icosahedral unit

Oxidation of pyrrolidine

Active sites

Catalytic activity

ABSTRACT

Atomically precise gold cluster catalysts have emerged as a new frontier in catalysis science, owing to their unexpected catalytic properties. In this work, we explore the evolution of the catalytic activity of clusters formed by the structural fusion of icosahedral Au₁₃ units, namely Au₂₅(SR)₁₈, Au₃₈(SR)₂₄, and Au₂₅(PPh₃)₁₀(SC₂H₄Ph)₅Cl₂, in the oxidation of pyrrolidine to γ -butyrolactam. We demonstrate that the structural fusion of icosahedral Au₁₃ units, forming vertex-fused (vf), face-fused (ff), and body-fused (bf) clusters, can induce a decrease in the catalytic activity in the following order: Au_{bf} > Au_{ff} > Au_{vf}. The structural fusion of icosahedral Au₁₃ units in the clusters does not distinguish the adsorption modes of pyrrolidine over the three clusters from each other, but modulates the chemical adsorption capacity and electronic properties of the three clusters, which is likely to be the key reason for the observed changes in catalytic reactivity. Our results are expected to be extendable to study and design atomically defined catalysts with elaborate structural patterns, in order to produce desired products.

© 2021, Dalian Institute of Chemical Physics, Chinese Academy of Sciences.

Published by Elsevier B.V. All rights reserved.

Recently, ligand-capped Au_n clusters (*n* = number of gold atoms, ranging from a dozen to hundreds) with precise atomic structures have attracted considerable interest. Significant advances have been made in the synthesis and unambiguous structural determination of atomically precise Au_n clusters [1–4]. These clusters are unique and substantially different from their larger nanoparticle counterparts (typically 3–100 nm), as the former exhibit a range of fascinating optical, electronic, and magnetic properties [5], which are not observed in the latter. Small Au_n clusters (relative to Au₁₄₄, that is, smaller than 1.7 nm) exhibit molecular-like behavior such as single-electron transitions or excitons; relatively larger ones (between Au₁₄₄ and Au₃₃₃, i.e., 1.7–2.3 nm) exhibit intermediate properties between molecular and metallic behavior [6–8]; clusters of size larger than that of Au₃₃₃ (> 2.3 nm) can be classified as metallic. Overall, the molecular or non-metallic behav-

ior of Au_n clusters in excitonic and transition regimes is particularly important in catalysis, where these systems often display unexpected catalytic performances in some important chemical reactions, and exhibit a clear correlation between properties and structure [9–13].

More importantly, precisely controlling the structure of clusters has proved to be a valuable strategy to improve catalytic activity and tune product selectivity. For example, although Au₂₈(SPh-tBu)₂₀ and Au₂₈(S-c-C₆H₁₁)₂₀ have the same Au₂₀ core, the different surface structure of the two clusters can result in different catalytic activity and selectivity toward CO₂ hydrogenation [14]. The structural evolution from the mono-icosahedral [Au₁₃(PPh₃)₁₀X₂]³⁺ to the bi-icosahedral [Au₂₅(PPh₃)₁₀(SC₂H₄Ph)₅X₂]²⁺ and even to the tri-icosahedral [Au₃₇(PPh₃)₁₀(SC₂H₄Ph)₁₀X₂]⁺ cluster also illustrates the structure-dependent effects on CO oxidation [15]. Even the replace-

* Corresponding author. Tel: +86-25-89681696; E-mail: zhuyan@nju.edu.cn

This work was supported by the National Natural Science Foundation of China (21773109, 91845104).

DOI: 10.1016/S1872-2067(20)63659-2 | <http://www.sciencedirect.com/science/journal/18722067> | Chin. J. Catal., Vol. 42, No. 2, February 2021

ment of only a central atom of a cluster by a foreign atom can have substantial influence on the catalytic activity [16–18]. Therefore, the study of atomically precise clusters in catalytic applications opens a new avenue for the design of catalysts with improved efficiency, based on clusters with precise structures. Herein, we explore the evolution of the catalytic activity of clusters formed by the structural fusion of icosahedral Au₁₃ units in different modes, namely, Au₂₅(SR)₁₈, Au₃₈(SR)₂₄, and Au₂₅(PPh₃)₁₀(SC₂H₄Ph)₅Cl₂, by evaluating their performance in the oxidation of pyrrolidine to γ -butyrolactam.

The compositions of the three clusters, as determined by electrospray ionization mass spectrometry (ESI-MS), were Au₂₅(SR)₁₈, Au₃₈(SR)₂₄, and Au₂₅(PPh₃)₁₀(SC₂H₄Ph)₅Cl₂ (Fig. 1(d)–(f)). The frameworks of the three clusters are shown in Figs. 1(a)–(c). The Au₂₅(PPh₃)₁₀(SC₂H₄Ph)₅Cl₂ cluster exhibits a bi-icosahedral structure obtained by the fusion of two icosahedral Au₁₃ units joined by sharing one vertex gold atom (Fig. 1(a)), denoted as Au_{vf} (vf: vertex-fused). The Au₃₈(SC₂H₄Ph)₂₄ is based on a face-fused (ff) bi-icosahedral Au₂₃ core capped by a second shell comprising the remaining 15 gold atoms. The two icosahedra are fused together by sharing a common Au₃ face, yielding the Au₂₃ core (Fig. 1(b)), denoted as Au_{ff}. The

Au₂₅(SC₂H₄Ph)₁₈ cluster features an icosahedral Au₁₃ core encapsulated by an external gold shell consisting of the remaining 12 gold atoms; in this case, body fusion (bf) results in the formation of an icosahedral Au₁₃ core (Fig. 1(c)), named Au_{bf}. As we can see, the structural fusion of icosahedral Au₁₃ units increases with the growth of the sharing Au atom.

The structural fusion of icosahedral Au₁₃ units in the three clusters results in changes in optical and electronic properties. Fig. S1 shows that the UV-vis optical bands of Au_{bf} are observed at 400, 447, and 683 nm. In the case of Au_{vf}, the UV-vis absorbance peaks appear at 320, 416, and 677 nm, whereas the absorbance peaks of Au_{ff} are found at 1050, 750, 620, 520, and 490 nm. The UV spectra of the three clusters are in good agreement with previously reported data [19–21]. Differential potential voltammetry curves of the Au_{vf}, Au_{ff}, and Au_{bf} clusters at room temperature are shown in Fig. S2. For the Au_{ff} clusters, the first oxidation and reduction waves are found at +0.48 and –0.71 V (vs. a quasi-reference Ag electrode), respectively. This reveals that the electrochemical energy gap of Au_{ff} is ~ 1.2 eV, which is clearly different from that of Au_{bf} (~ 1.63 eV) and Au_{vf} (~ 1.54 eV). After subtracting the charging energy, these values were converted to actual HOMO-LUMO gaps of 1.0, 1.34, and

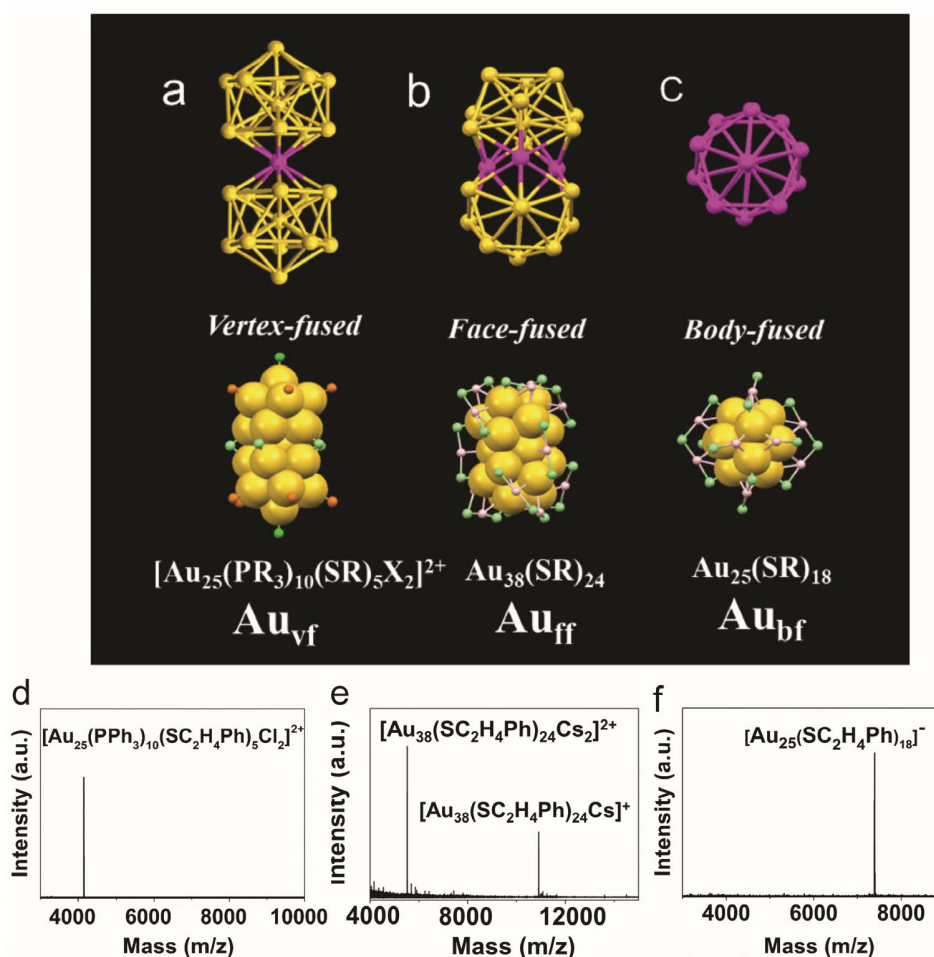


Fig. 1. Structural fusion of icosahedral Au₁₃ units: (a) vertex-fused bi-icosahedral Au₂₅, (b) face-fused bi-icosahedral Au₃₈, and (c) body-fused icosahedral Au₂₅. C and H atoms are omitted for clarity. Color labels: yellow, pink, and magenta: gold; light green: S; dark green: Cl; orange: P. ESI-MS profiles of (d) Au_{vf}, (e) Au_{ff}, and (f) Au_{bf}.

1.21 V for Au_{ff}, Au_{bf}, and Au_{vf}, respectively [11,12,2]. These measured gaps are close to the optical energy gaps of Au_{ff} (0.92 eV), Au_{vf} (1.31 eV), and Au_{bf} (1.18 eV), respectively, obtained from the UV-vis spectra by extrapolation to zero absorbance (Fig. S1). The results show that the three gold clusters exhibit non-metallic behavior.

An important question is whether the structural fusion of icosahedral Au₁₃ units can affect the catalytic activity and, if so, how it can control the catalytic process. In order to address these fundamental questions, the reaction of pyrrolidine with O₂ to form γ -butyrolactam was selected to evaluate the catalytic activity of the Au_{bf}, Au_{ff}, and Au_{vf} clusters. First, we examined the catalytic performances of the three clusters loaded on different supports (SiO₂, CeO₂, Al₂O₃, and P25) in the pyrrolidine oxidation (Fig. S3). Among the different supports examined, CeO₂ was the best choice; in this case, upon the introduction of O₂ into the reaction system, the oxygen vacancies of CeO₂ can facilitate the oxidation reaction [22]. Note that CeO₂ alone had limited activity (Table S1, entry 1), while the pure ligands had no activity (Table S1, entries 3–4). These results indicate that the catalytic performance was mainly determined by the gold sites, rather than the ligands or supports.

Among the three catalysts, Au_{bf}/CeO₂ exhibited the highest activity (~ 80% conversion), while Au_{vf}/CeO₂ gave rise to the lowest activity (~ 40% conversion). The catalytic activity de-

creased in the order Au_{bf} > Au_{ff} > Au_{vf} (Fig. 2(a)). The superior activity of Au_{bf} over Au_{vf} and Au_{ff} was also reflected by the reaction rates of pyrrolidine over the three catalysts. The corresponding kinetic profiles for the reaction, shown in Fig. 2(b), not only indicate that the pyrrolidine oxidation was approximately a first-order reaction, but also confirm that the reaction rate constant of pyrrolidine oxidation over Au_{bf} was approximately 1.5–2 times higher than those of the Au_{vf} and Au_{ff} reaction systems ($29.84 \times 10^{-3} \text{ h}^{-1}$ for Au_{bf}, $14.79 \times 10^{-3} \text{ h}^{-1}$ for Au_{vf}, and $17.21 \times 10^{-3} \text{ h}^{-1}$ for Au_{ff}). The activation energy (E_a) for Au_{bf} was found to be $34.67 \text{ kJ}\cdot\text{mol}^{-1}$, which was lower than those of other two catalysts (Au_{vf}: $66.26 \text{ kJ}\cdot\text{mol}^{-1}$; Au_{ff}: $52.71 \text{ kJ}\cdot\text{mol}^{-1}$) (Fig. 2(c)). Notably, the influence of the different ligands of Au_{bf} (Fig. S4) on the pyrrolidine conversion, as shown in Fig. 2(d), indicates that the pyrrolidine conversion varied with the chain length of the ligands, with the highest value observed in the case of the Au_{bf}-*n*-butyl mercaptan, followed by Au_{bf}-1-octanethiol and then Au_{bf}-1-dodecanethiol. The conversion was observed to increase with decreasing chain length, which suggests that it is much easier for the pyrrolidine molecules to access the surface gold sites because of the smaller steric hindrance compared to that of long-chain thiolate molecules [23].

Notably, the three catalysts only yielded trace amounts of γ -butyrolactam in air (0.4 MPa; Table S1, entries 5–7), while an

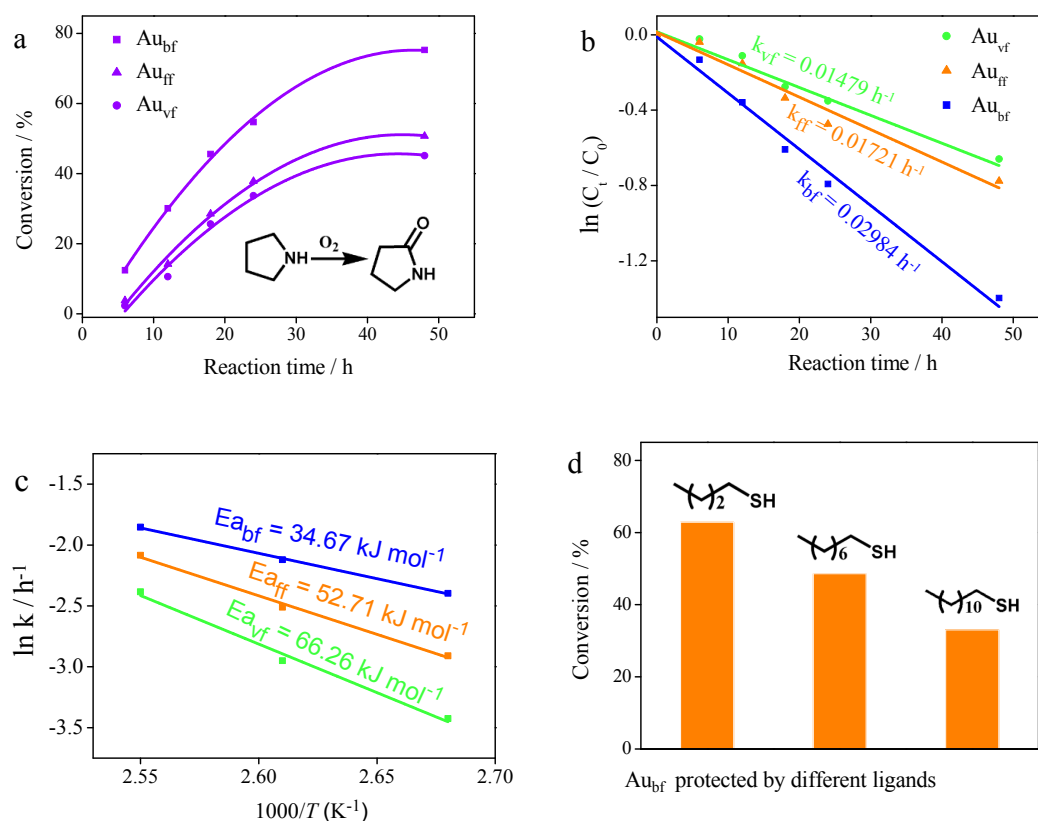


Fig. 2. (a) Catalytic oxidation of pyrrolidine over Au_{vf}, Au_{ff}, and Au_{bf} catalysts. Reaction conditions: catalyst (100 mg, 2 wt% Au), pyrrolidine (0.44 mmol), O₂ (0.4 MPa), *n*-butanol/H₂O (4.5 mL/0.5 mL), 85 °C for different reaction times. (b) Linear dependence of $\ln(C_t/C_0)$ on reaction time for the oxidation of pyrrolidine over Au_{vf}, Au_{ff}, and Au_{bf} catalysts. (c) Arrhenius plot for pyrrolidine oxidation. (d) Conversion of pyrrolidine over Au_{bf} catalysts protected by different thiolate groups (*n*-butyl mercaptan, 1-octanethiol, and 1-dodecanethiol) (48 h).

increasing yield of product was obtained in pressurized air (1 MPa; Table S1, entries 8–10). The reaction did not proceed under N₂ atmosphere (1 MPa; Table S1, entries 11–13), indicating that O₂ was the oxidant in the reaction. Furthermore, we studied the effect of H₂O on the catalytic performances. As shown in Fig. S5, the results show that a very low conversion of pyrrolidine (< 10%) was obtained when H₂O was absent. An increase in the amount of H₂O led to an increase in the conversion of pyrrolidine. When the H₂O amount reached 0.75–1 mL, the conversion decreased, due to ring-opening hydrolysis of γ -butyrolactam. This suggests that water was necessary for this oxidation reaction.

Under the optimized reaction conditions, we also extended the substrate scope for the reaction. As shown in Table S2, five-, six-, and seven-membered cyclic amines could be oxidized to produce the corresponding amides. In these reactions, Au_{bf} still showed superior activity to Au_{vf} and Au_{ff}. Furthermore, the clusters exhibited catalytic stability, up to a certain extent (Fig. S6). The UV-vis spectra of the spent clusters dissolved in CH₂Cl₂ indicate that the clusters showed no dramatic changes after the catalytic reactions (Fig. S7). The transmission electron microscopy (TEM) images show that the clusters exhibited no obvious aggregation during the reactions (Fig. S8).

Fourier-transform infrared (FT-IR) spectra of CO adsorbed onto the three catalysts were obtained to probe the nature of the available Au sites. As shown in Fig. 3(a), the band at 2168 cm⁻¹ is assigned to gaseous CO and that at 2117 cm⁻¹ is attributed to CO molecules adsorbed onto the Au ^{δ +} (0 < δ < 1) sites [24–26]. As we can see, CO was only weakly adsorbed on surface Au cations, but the relative intensities of CO adsorbed on the three samples were different, and the chemical adsorption capacity of CO on Au sites followed the order Au_{bf} > Au_{ff} > Au_{vf}. It was proposed that the different chemical adsorption capacities of CO on the clusters might account for the different reactivity of the three catalysts. There were indications of a higher number of catalytic active sites on the Au_{bf} catalyst, followed by Au_{ff} and then Au_{vf}. Fig. 3(b) shows that the peaks at 2158 and 2117 cm⁻¹ decreased in intensity with increasing chain length of the ligands, which reveals that the longer alkyl

chains led to a higher hindrance, making it more difficult for CO to access the surface Au sites. Therefore, these observations were in line with the consequence of the catalytic activities, supporting the observed evolution of the activity in the pyrrolidine oxidation.

To obtain further insight into the reaction mechanism, the adsorption of pyrrolidine onto the three clusters was investigated *via* FT-IR spectroscopy. Fig. 4(a) shows that the peaks of the –NH stretching vibration at 3325 cm⁻¹ of pyrrolidine adsorbed onto the clusters could hardly be seen. The comparison with the IR spectra of pure pyrrolidine and of the three isolated clusters (Fig. S9) reveals that the –NH group interacted with the clusters, and the H atom of the –NH group was mostly removed from the amines and further activated. This indicates that the adsorption of pyrrolidine on the three clusters involved its dehydrogenation process [9]. The X-ray photoelectron spectroscopy (XPS) analysis of the three clusters further highlights the changes in electronic structure upon the structural fusion of Au₁₃ units. As clearly shown in Fig. 4(b) and Table S3, the shift of the Au 4*f* binding energies of the Au_{bf} cluster was more positive than those of Au_{ff} and Au_{vf}. The XPS data show that the Au 4*f* binding energies of Au_{bf} were positively shifted, compared to those of Au_{ff} and Au_{vf}. Au⁰ and Au⁺ species were detected in the Au 4*f* spectra of the three nanoclusters. In particular, the Au⁺ species appeared on the surface of nanoclusters, mainly due to the electron donation from the surface Au atoms to the ligands. The molar ratio of Au⁺ to Au⁰ was 0.7 for Au_{bf}, 0.63 for Au_{ff}, and 0.51 for Au_{vf}, revealing that Au_{bf} had a more positive charge in comparison with Au_{ff} and Au_{vf}. When O₂ was used as an oxidant, it could directly attack the Au atoms to form the Au_{cluster}–O₂(ad) species. With respect to the NH activation of pyrrolidine, the presence of Au⁺ among the surface Au atoms could substantially activate the nucleophilic –NH group of pyrrolidine, since the surface Au⁺ species are electrophilic [27]. Then, the activated –NH groups reacted with the O₂(ad) species on the surface of the Au clusters. Thus, the more positive charge on the surface Au atoms can lead to a higher catalytic ability to activate the nucleophilic –NH group. On the basis of the XPS data, the activity decreased in the order

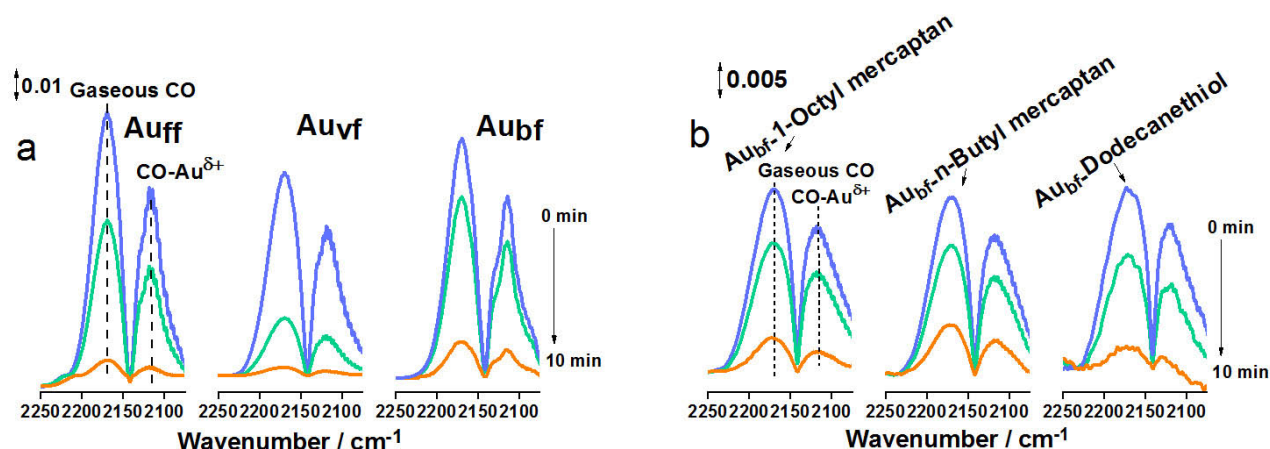


Fig. 3. (a) *In situ* FT-IR spectra of CO adsorbed onto the Au_{vf}, Au_{ff}, and Au_{bf} clusters; (b) *In situ* FT-IR spectra of CO adsorbed onto the Au_{bf} clusters capped by different alkanethiol ligands.

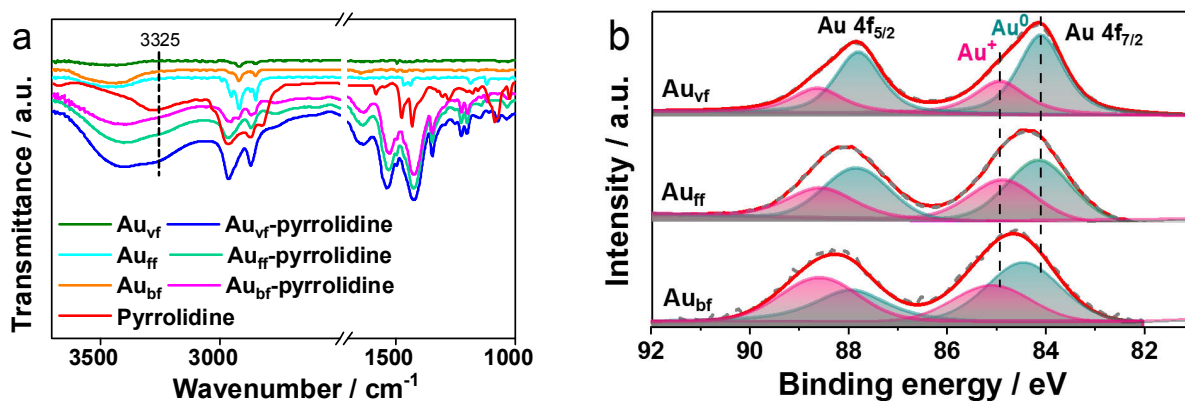


Fig. 4. (a) FT-IR spectra of adsorbed species over the catalysts in the presence of pyrrolidine; (b) XPS profiles of Au_{vf}, Au_{ff}, and Au_{bf} clusters.

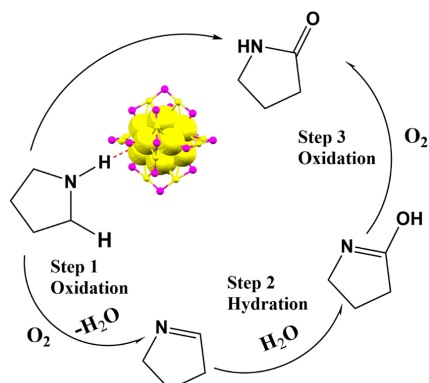
Au_{bf} > Au_{ff} > Au_{vf}, which is essentially in agreement with the experimental results.

Overall, we proposed a possible mechanism for pyrrolidine oxidation on gold clusters, based on the oxidation/hydration/oxidation sequence illustrated in Scheme 1. In the first step, O₂ is dissociated into O atoms on the gold cluster sites and the β-hydrogen is transferred to the gold sites with release of H₂O, to give the imine product. In the second and third steps, the imine is hydrolyzed and then oxidized to produce γ-butyrolactam.

In summary, we reported the influence of the structural fusion of icosahedral Au₁₃ units on the catalytic reactivity in the oxidation of pyrrolidine to produce γ-butyrolactam. The structural fusion of icosahedral Au₁₃ units in the clusters does not distinguish the adsorption modes of pyrrolidine over the three clusters from each other, but modulates the chemical adsorption capacity and electronic properties of the clusters, which is likely to be the reason for the observed changes in catalytic reactivity. This work can be extended to explore the wider catalytic application of non-metallic catalysts with appropriate structural patterns to produce desired products.

References

[1] T. Higaki, Q. Li, M. Zhou, S. Zhao, Y. W. Li, S. Li, R. C. Jin, *Acc. Chem.*



Scheme 1. Proposed mechanism of pyrrolidine oxidation on gold clusters.

Res., **2018**, 51, 2764–2773.

- [2] B. Nieto-Ortega, T. Bürgi, *Acc. Chem. Res.*, **2018**, 51, 2811–2819.
- [3] P. X. Liu, R. X. Qin, G. Fu, N. F. Zheng, *J. Am. Chem. Soc.*, **2017**, 139, 2122–2131.
- [4] I. Chakraborty, T. Pradeep, *Chem. Rev.*, **2017**, 117, 8208–8271.
- [5] S. B. Tian, L. W. Liao, J. Y. Yuan, C. H. Yao, J. S. Chen, J. L. Yang, Z. K. Wu, *Chem. Commun.*, **2016**, 52, 9873–9876.
- [6] Z. Lei, Q. M. Wang, *Coord. Chem. Rev.*, **2019**, 378, 382–394.
- [7] R. Ishida, S. Arai, W. Kurashige, S. Yamazoe, K. Koyasu, Y. Negishi, T. Tsukuda, *Chin. J. Catal.*, **2016**, 37, 1656–1661.
- [8] H. J. Chen, C. Liu, M. Wang, C. F. Zhang, G. Li, F. Wang, *Chin. J. Catal.*, **2016**, 37, 1787–1793.
- [9] Y. Y. Liu, X. Q. Chai, X. Cai, M. Y. Chen, R. C. Jin, W. D. Ding, Y. Zhu, *Angew. Chem. Int. Ed.*, **2018**, 57, 9775–9779.
- [10] Y. Zhu, H. F. Qian, A. Das, R. C. Jin, *Chin. J. Catal.*, **2011**, 32, 1149–1155.
- [11] Y. W. Zhang, P. Song, T. Chen, X. D. Liu, T. Chen, Z. M. Wu, Y. Wang, J. P. Xie, W. Lin, *Proc. Natl. Acad. Sci. USA*, **2018**, 115, 10588–10593.
- [12] Y. Zhu, H. F. Qian, B. A. Drake, R. C. Jin, *Angew. Chem. Int. Ed.*, **2010**, 49, 1295–1301.
- [13] Y. Tan, H. Liu, X. Y. Liu, A. Q. Wang, C. J. Liu, T. Zhang, *Chin. J. Catal.*, **2018**, 39, 929–936.
- [14] J. Xu, M. Chen, Y. Zhu, *Chem. Eur. J.*, **2019**, 25, 9185–9190.
- [15] S. H. Xie, H. Tsunoyama, W. Kurashige, Y. Negishi, T. Tsukuda, *ACS Catal.*, **2012**, 2, 1519–1523.
- [16] Z. B. Gan, N. Xia, Z. K. Wu, *Acc. Chem. Res.*, **2018**, 51, 2774–2783.
- [17] Z. M. Li, X. J. Yang, C. Liu, J. Wang, G. Li, *Prog. Nat. Sci.*, **2016**, 26, 477–482.
- [18] K. Kwak, Q. Tang, M. Kim, D. E. Jiang, D. Lee, *J. Am. Chem. Soc.*, **2015**, 137, 10833–10840.
- [19] M. Z. Zhu, E. Lanni, N. Garg, M. E. Bier, R. C. Jin, *J. Am. Chem. Soc.*, **2008**, 130, 1138–1139.
- [20] H. F. Qian, Y. Zhu, R. C. Jin, *ACS Nano*, **2009**, 3, 3795–3803.
- [21] H. F. Qian, M. Z. Zhu, E. Lanni, Y. Zhu, M. E. Bier, R. C. Jin, *J. Phys. Chem. C*, **2009**, 113, 17600–17603.
- [22] A. Abad, P. Concepcion, A. Corma, H. García, *Angew. Chem. Int. Ed.*, **2005**, 44, 4066–4069.
- [23] A. Shivhare, S. J. Ambrose, H. Zhang, R. W. Purves, R. W. J. Scott, *Chem. Commun.*, **2013**, 49, 276–278.
- [24] Z. Wu, D. E. Jiang, A. K. P. Mann, D. R. Mullins, Z. Qiao, L. F. Allard, C. Zeng, R. Jin, S. H. Overbury, *J. Am. Chem. Soc.*, **2014**, 136, 6111–6122.

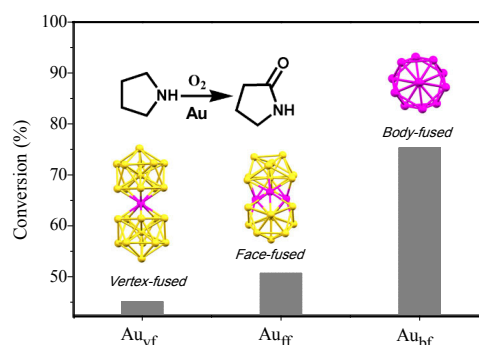
Graphical Abstract

Chin. J. Catal., 2021, 42: 245–250 doi: 10.1016/S1872-2067(20)63659-2

Evolution of catalytic activity driven by structural fusion of icosahedral gold cluster cores

Dan Yang, Yan Zhu*
Nanjing University

Atomically precise gold cluster catalysts have emerged as a new frontier in catalysis science and exhibited unexpected catalytic properties. Here, we demonstrate that the structural fusion of icosahedral Au₁₃ cores to form vertex-fused (vf), face-fused (ff), and body-fused (bf) structures can control the catalytic activity of the clusters.



[25] Z. L. Wu, D. E. Jiang, A. K. P. Mann, D. R. Mullins, Z. A. Qiao, L. F. Allard,

C. J. Zeng, R. C. Jin, S. H. Overbury, *Nano Lett.*, **2016**, 16, 6560–6567.

[26] F. Boccuzzi, A. Chiorino, M. Manzoli, P. Lu, T. Akita, S. Ichikawa, M.

Haruta, *J. Catal.*, **2001**, 202, 256–267.[27] Q. L. Wang, K. Q. Shen, M.Y. Chen, Y. Zhu, *Nanoscale*, **2019**, 11, 13767–13772.

金团簇二十面体结构融合过程中其催化活性的演变

杨丹, 祝艳*

南京大学化学化工学院, 江苏南京210093

摘要: 近年来, 由有机配体保护的原子精确金属团簇在合成方面已取得了重要进展, 其独特的原子结构对一些化学反应产生独特的催化效果. 原子精确的团簇催化剂明显不同于纳米颗粒催化剂和单原子催化剂, 是一种关联均相和多相的、原子数目确定、尺寸均一、结构精确的新型催化剂. 从原子尺度上精确构筑团簇催化剂, 探究亚纳米尺度的微观结构对催化性能的影响, 为常规催化剂所未能解决的关键科学问题提供解决的机会, 为在分子尺度上揭示催化作用机制以及准确关联催化剂结构与催化性能提供新的研究体系, 具有重要的科学研究意义. 本文设计和使用了三种结构精确的金团簇催化剂, 即 Au₂₅(PPh₃)₁₀(SC₂H₄Ph)₅Cl₂, Au₃₈(SC₂H₄Ph)₂₄和 Au₂₅(SC₂H₄Ph)₁₈, 分别由二十面体结构的 Au₁₃单元通过中心顶点融合、面融合、体相融合形成的(简称为 Au_{vf}、Au_{ff}和 Au_{bf}), 详细研究了这三个金团簇催化剂在二十面体 Au₁₃单元的结构融合过程中, 其催化活性的演变规律. 在催化吡咯烷与 O₂ 反应制备 γ -丁内酰胺反应中, 金团簇催化剂的催化活性顺序为 Au_{bf} > Au_{ff} > Au_{vf}, 表明这三个金团簇中 Au₁₃单元的结构随着点、面、体的融合, 其催化活性随之增加. 同时研究发现, 对于同一个 Au 团簇催化剂, 其表面硫醇配体的烷基链越短, 其催化活性越高, 这主要是由于短链硫醇分子的空间位阻较小, 吡咯烷分子更容易进入催化剂的金表面, 接触到活性位点, 进行催化反应. 实验表明, 三个团簇金原子均带正电荷, 正价金物种可能是催化吡咯烷与 O₂ 反应的催化活性物种. 研究发现, Au_{bf} 团簇表面的活性位数目高于 Au_{ff} 和 Au_{vf} 团簇的, 因此 Au_{bf} 的催化活性最高; 同时, 团簇表面配体的烷基链越短, 其表面活性位数目也越多, 这也进一步解释了表面硫醇配体的烷基链越短, 其相应的金团簇催化剂的催化活性越高的原因. 吡咯烷与 O₂ 在金团簇上反应的可能路径为 O₂ 在 Au 活性位上裂解的 O 原子和吡咯烷 β -H 转移至 Au 活性位的 β -H 反应脱水后形成亚胺, 亚胺经过水解进一步氧化得到产物. 这项研究将为在原子层次上调变金属团簇催化剂的结构进而改变其催化性能提供新的思路, 对精准设计和构筑高效催化剂具有一定的科学指导意义.

关键词: 金团簇; 结构融合; 二十面体结构; 吡咯烷氧化; 活性位点; 催化活性

收稿日期: 2020-04-18. 接受日期: 2020-05-21. 出版日期: 2021-02-05.

*通讯联系人. 电话: (025)89681696; 电子信箱: zhuyan@nju.edu.cn

基金来源: 国家自然科学基金(21773109, 91845104).

本文的电子版全文由 Elsevier 出版社在 ScienceDirect 上出版 (<http://www.sciencedirect.com/science/journal/18722067>).